3.8 Gb/s PAM-4 UOWC System Over a 2-m Underwater Channel Enabled by a Single-Pixel 175-μm GaN-Based Mini-LED

Chao Zhang, Zixian Wei, Xueyang Li, *Member, IEEE*, Yibin Li, *Graduate Student Member, IEEE*, Lei Wang, *Member, IEEE*, Lai Wang, H. Y. Fu, *Senior Member, IEEE*, and Yanfu Yang, *Senior Member, IEEE*

***Abstract*—Blue/green light-emitting diodes (LEDs) have been studied extensively in medium/short-distance underwater optical wireless communication (UOWC), while available commercial bandwidth-limited LEDs cannot support the increased capacity. In this work, a 175-μm blue mini-LED with a high 3 dB modulation bandwidth of 580 MHz was designed and employed to implement a high-speed UOWC system to improve the bandwidth while maintaining high emitting optical power. As a result, we achieve the data rate of 3.8 Gb/s and the rate-distance product of 7.6 Gb/s·m of the PAM-4 signal with the 3.7e-3 bit error rate (BER) over the 2-m underwater channel by using a single-pixel 175-μm GaN-based mini-LED and an avalanche photodiode (APD). To the best of our knowledge, it is the highest rate-distance product among the UOWC systems based on a single-pixel LED and a single APD. In addition, we design multiple sets of comparison experiments to provide a comprehensive investigation regarding channel loss, transmission capacity, and computation complexity between the UOWC system with and without water.**

***Index Terms*—Mini-LED, PAM-4, UOWC, APD.**

I. Introduction

HIGH speed communication systems are required for underwater equipment to facilitate more convenient use of marine resources [1]. Submarine optical cables allow high-capacity connections yet at the cost of expensive deployment and maintenance [2]. Underwater acoustic communication has minimal data rates due to small system bandwidth (usually several kHz) in addition to high latency due to a slow propagation speed of acoustic waves [3]. Underwater RF communication, on the other hand, requires complex antenna designs with high emitting power [1]. Recently, short-reach underwater optical wireless communication (UOWC) has attracted attention because of its advantages, including high speed, low latency, low implementation cost, high security [4]. Since seawater has a low-attenuation window in the blue-green band spectrum (450 nm $\sim$ 550 nm), blue/ green laser diodes (LD) and light-emitting diodes (LED) are the most commonly used light sources for UOWC [5]. Typically, LD with high bandwidth ($>$ 1 GHz) and small divergence angle ($\sim 0.01°$) are suitable for high-capacity optical links over a relatively long distance [4]. C. Li *et al.* demonstrate a high-speed real-time data rate of 25 Gb/s based on non-return-to-zero on–off-keying (NRZ-OOK) with bit error rate (BER) of 3×10^{-9} over 5-m in highly turbid harbor water by use of a 680-nm red-light vertical-cavity surface-emitting laser (VCSEL) [6]. H. Chen *et al.* transmitted a 2 Mb/s OOK signal over 117-m using a blue LD and a single-photon avalanche diode (SPAD) receiver [7]. Compared to LDs, LEDs have lower cost, lower power consumption, longer lifetime, and are widely used for illumination due to their safety for human eyes [2]. However, the commercial LEDs have limited modulation bandwidth and a large divergence angle, which constrains the capacity of the UWOC. For decreasing the influence of the limited bandwidth of the transmitter, mini-LEDs or micro-LEDs are proposed to obtain a higher modulation bandwidth by reducing the carrier lifetime and resistance-capacitance (RC) delay. In the past decade, mini-LEDs or micro-LEDs have been intensively investigated for the UOWC system. Y. Zhou *et al.* realized transmission of a 5.17 Gb/s bit-loading-discrete multitone (bit-loading-DMT) signal over a 1.2-m underwater channel by using a self-designed common-anode GaN-based five-primary-color LED [8]. G. N. Arvanitakis *et al.* demonstrate the transmission of a 3.4 Gb/s orthogonal frequency division multiplexing (OFDM) signal underwater over a distance of 4.5 m using series-connected micro-LED arrays [9]. Z. Wei *et al.* fabricated and packaged a 75-μm blue micro-LED with a high modulation bandwidth up to 1.03 GHz. A data rate of 2 Gb/s with a BER of 2.03×10^{-3}

Manuscript received December 15, 2021; revised January 15, 2022; accepted January 19, 2022. Date of publication January 31, 2022; date of current version April 22, 2022. This work was supported in part by the National Key Research and Development Program of China under Grant 2018YFB0406702, in part by the National Natural Science Foundation of China under Grants 61822404 and 61974080, in part by the Science, Technology and Innovation Commission of Shenzhen Municipality under Grants JCYJ20190806142407195, JCYJ20210324131408023, JCYJ20180507183815699, and WDZC20200820160650001, and in part by the Guangdong Basic and Applied Basic Research Foundation under Grant 2021A1515011450. *(Corresponding author: Yanfu Yang.)*

Chao Zhang and Yanfu Yang are with the Department of Electronic and Information Engineering, Harbin Institute of Technology, Shenzhen, Shenzhen, Guangdong 518055, China (e-mail: 19s052002@stu.hit.edu.cn; yangyanfu@hit.edu.cn).

Zixian Wei, Yibin Li, and H. Y. Fu are with Tsinghua Shenzhen International Graduate School and Tsinghua-Berkeley Shenzhen Institute, Tsinghua University, Shenzhen, Guangdong 518055, China (e-mail: weizx17@tsinghua.org.cn; liyibin21@mails.tsinghua.edu.cn; hyfu@sz.tsinghua.edu.cn).

Xueyang Li is with Photonic Systems Group, Department of Electrical and Computer Engineering, McGill University, Montréal, QC H3A 0E9, Canada (e-mail: xueyang.li@mail.mcgill.ca).

Lei Wang and Lai Wang are with the Department of Electronic Engineering, Tsinghua University, Beijing 100084, China (e-mail: l-wang16@mails.tsinghua.edu.cn; wanglai@tsinghua.edu.cn).

Digital Object Identifier 10.1109/JPHOT.2022.3145188

TABLE I
SUMMARY OF COMMUNICATION PERFORMANCES OF SOME RECENT UOWC SYSTEMS

Year	Reference	LED types	Receiver	Modulation format	Data rate (Gb/s)	BER	Distance (m)
2017	[11]	2 blue LEDs	2 PINs	4QAM-OFDM	0.033	< 7% FEC	2.0
2017	[12]	Blue μLED	PIN/APD	NRZ-OOK	0.8 0.2	1.3×10^{-3} 3.0×10^{-6}	0.6 5.4
2018	[13]	56 blue LEDs	PMT	OFDM	0.205	< 7% FEC	10
2018	[14]	RGBYC LED	PIN	PAM-8	1.5	< 7% FEC	1.2
2018	[15]	2 blue LEDs	MPPC	PAM-4	0.012288	2.9×10^{-3}	2.0
2018	[16]	Blue LED	PIN	8QAM-DMT	1.62	< 7% FEC	1.2
2018	[17]	Green LED	2 PINs	64QAM-DMT	2.175	< 7% FEC	1.2
2019	[8]	RGBYC LED	PIN	64QAM-DMT	15.17	< 7% FEC	1.2
2019	[18]	Blue LED	2×2 PINs	32QAM-DMT	1.8	< 7% FEC	1.2
2019	[19]	Blue LED	PIN	Real-time DMT	2.34	3.5×10^{-3}	1.2
2019	[20]	Blue HV-LED	PIN	16QAM-OFDM	3	< 7% FEC	1.2
2020	[9]	6 μLEDs	PIN	OFDM	4.92	1.5×10^{-3}	1.5
2020	[10]	QD blue μLED	APD	NRZ-OOK	2	2.0×10^{-3}	2
2021	**This works**	**Mini-LED**	**APD**	**PAM-4**	**3.8**	**< 7% FEC**	**2**

using an NRZ-OOK format over a 3-m air-underwater channel was achieved [10]. Quadrature-amplitude-modulation (QAM) OFDM modulation has shown excellent transmission performance in UOWC systems. However, it has the issues of the high peak-to-average power ratio (PAPR) and implementation complexity. In comparison, 4-ary pulse amplitude modulation (PAM-4) is an attractive format for the UOWC system due to its trade-off between system performance and implementation, which is also compatible with the existing short-range communications [21]. In the UOWC systems, two significant issues should be considered in practice: the bandwidth constraint of the photo-electric components and their nonlinearity. Various DSP techniques such as linear pre-equalization and nonlinear Volterra equalizer (VE) can resolve these two problems [22], [23]. Pre-equalization is applied at the transmitter to alleviate the inter symbol interference (ISI) due to limited system bandwidth. A simple digital linear pre-equalization technology was used to verify 400 Mb/s PAM-4 based on a blue LED [22]. An equalizer combined with noise-whitening post-filter plus maximum likelihood sequence detection (MLSD) was used to mitigate the system loss induced by the bandwidth limitation without the channel information [24]. In addition, the VE is used to mitigate the nonlinearity in the visible light communication system [23]. However, the most apparent issue of VE is its high computation complexity. Several schemes have been proposed to reduce the complexity, including the modified Gram-Schmidt (GS) orthogonal decomposition [25], $\ell 1$-regularization [26], and principal component analysis (PCA) [27].

Compared with other recent UOWC works based on a single-pixel LED shown in Table I, we achieve, to our knowledge, the highest data rate of 3.8 Gb/s and the highest rate-distance product of 7.6 Gb/s·m. Furthermore, to obtain the trade-off between the modulation bandwidth and optical power, a 175-μm 580 MHz blue mini-LED is designed and fabricated based on a standard *c*-plane, which is used as the optical source for a 2-m UOWC system. On the receiver side,

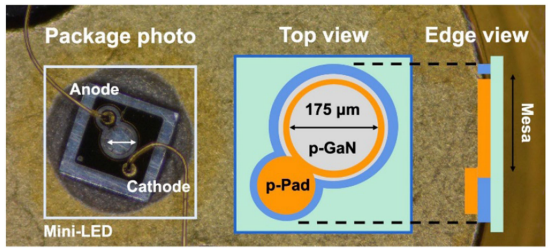

Fig. 1. The schematic of the LED chip and the photograph of the packaged blue mini-LED.

the BER can be significantly decreased by a low-complexity VE based on the targeted principal component analysis (TPCA) and adaptive noise-whitening post-filter with MLSD compared to the traditional feed-forward linear equalizer (LE)[27], [28]. In addition, the impact of the operating parameters, including the driving current of the mini-LED and the modulation depth (peak-to-peak voltage, Vpp) of the input RF signals, are characterized in detail to maximize the capacity of the UOWC system.

II. DEVICES AND EXPERIMENTAL SETUP

A. Design and Fabrication of Single-Pixel Mini-LED

Fig.1 shows the package photography of the 175-μm blue mini-LED and the active region formed with a diameter of 175-μm. The inset figures are the schematic diagrams of the top view and the edge view. Firstly, using metal-organic chemical vapor-phase deposition (MOCVD, 2000HT, Aixtron), the LED epitaxial plates were grown with a 430 μm thickness. Then the LED pattern was designed in the fabrication processing by wet etching. After that, by using dry etching inductively coupled plasma-reactive etching, the growth of the mesa of the mini-LED is completed. Our previous work has reported the growth techniques of the epitaxial wafer and the fabrication process of

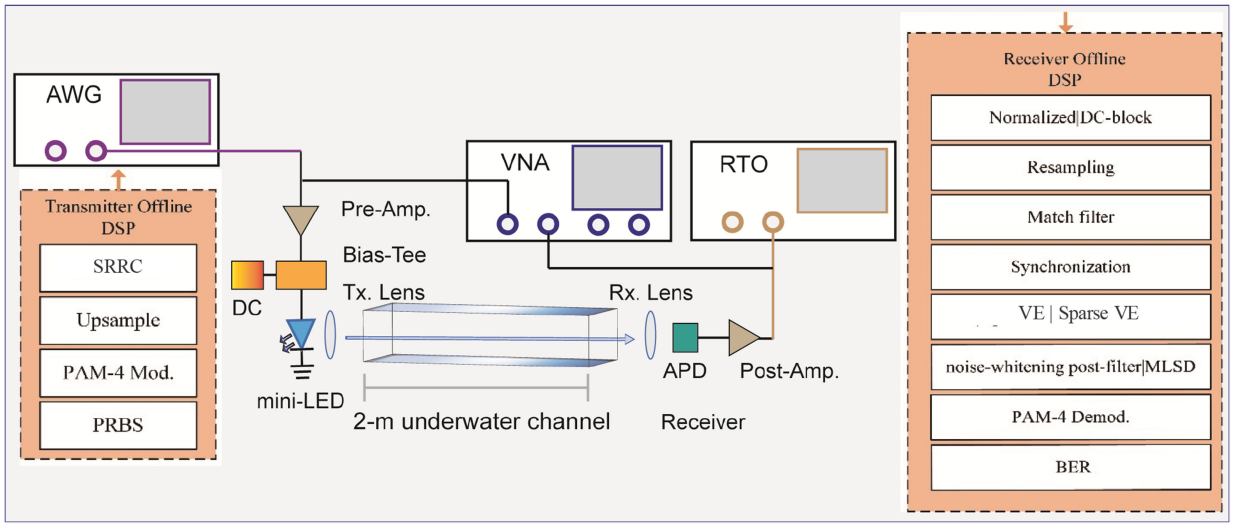

Fig. 2. Schematic diagram of the UOWC experimental setup with the offline VE. (AWG: arbitrary waveform generator; VNA: vector network analyzer; RTO: real-time oscilloscope; APD: avalanche photodiode.

the device [29], [30]. The magnified view in Fig. 1 shows a transistor-outline window-can (TO-CAN) package after fabrication of the mini-LED, which includes the anode and cathode.

Fig. 2 shows the PAM-4 UOWC system utilizing the packaged blue mini-LED over a 2-m underwater channel. The experimental system contains the offline DSP modules using MATLAB and the real-time light propagation link. Firstly, the binary pseudo-random code (PRBS) was generated and mapped into the PAM-4 sequence. Then the PAM-4 sequence was up-sampled and pulsed through a square-root raised-cosine (SRRC)filter with the roll-off factor (RF) of 0.1. Next, the generated waveform was imported into an arbitrary waveform generator (AWG, AWG7000A, Tektronix) to generate an electrical signal. Next, the electrical signal was amplified by an amplifier (SHF 100BP-ML) and loaded with a direct current (DC) component provided by a bias-tee (ZFBT-6GW+, Mini-circuit). Finally, this positive signal was injected into the packaged mini-LED. The generated PAM-4 optical signal was first passed through a convex lens to improve the directivity of the emitted beam and then transmitted through a 2-m water tank with water and without water, respectively. The OWC results are also presented here as a reference such that the impact of the channel loss on the achievable bit rate can be evaluated. The receiving lens focused the beam right on the center of the active area of a high-sensitivity silicon avalanche photodiode (APD) module (APD210, Menlo Systems), which converted the received optical signal into an electrical current. Finally, a real-time oscilloscope (RTO, DPO75902SX, Tektronix) collected the converted electrical signal, and the subsequent DSP modules processed the sampled signal.

The captured PAM-4 signal at the receiver was DC-blocked, normalized, re-sampled, and match filtered. Synchronization was obtained by a digital square and filter clock recovery algorithm. For a high-speed PAM-4 UOWC system, the linear impairment mainly comes from the limited bandwidth of opto-electronic components. The nonlinear impairment is primarily related to modulation nonlinearity introduced by mini-LED, nonlinear amplification or saturation distortion introduced by an electric amplifier, and signal-signal beating interference (SSBI) caused by APD, etc. [31]. In this work, to make a trade-off between the computation complexity and accuracy, three-order VE is adopted to compensate for the system's impairment [23]. To get the kernel coefficients of the VE, we used the training-symbol-based recursive least squares (RLS) algorithm. However, the 3-order VE has a significant number of coefficients which makes the VE quite complex. To reduce the complexity of the VE effectively, the TPCA is used to identify and remove less important kernel coefficients to implement a sparse VE [27]. The first order of VE is the traditional linear equalizer which can mitigate the linear impairment. Before the VE, the noise is white in the frequency domain; after the VE, a higher noise power at the high-frequency range is present. When compensating for the linear impairment, the VE enhances the in-band noise and colors it, degrading UOWC performance. A noise-whitening post-filter that consists of a finite impulse response (FIR) equalizer is used to whiten the colored noise. The autoregressive (AR) method based on Yule-Walker equations is used to get the kernel coefficients of the noise-whitening post-filter [28]. The kernel coefficients of noise-whitening post-filter can be expressed as (1):

$$\begin{bmatrix} 1 \\ w_1 \\ \vdots \\ w_i \end{bmatrix} = \begin{bmatrix} R(0) & R(1) & \cdots & R(i) \\ R(1) & R(0) & \cdots & R(i-1) \\ \vdots & \vdots & \ddots & \vdots \\ R(i) & R(i-1) & \cdots & R(0) \end{bmatrix}^{-1} \begin{bmatrix} R(0) \\ 0 \\ \vdots \\ 0 \end{bmatrix} \tag{1}$$

where $R(i)$ is the autocorrelation function of the noise shown in (2).

$$R(i) = \sum_{k} (s(k) - d(k)) \cdot (s(k+i) - d(k+i)) \tag{2}$$

where $s(k)$ is the k_{th} sample of the input signal to the noise-whitening post-filter, $d(k)$ is the decision of the $s(k)$. The signal

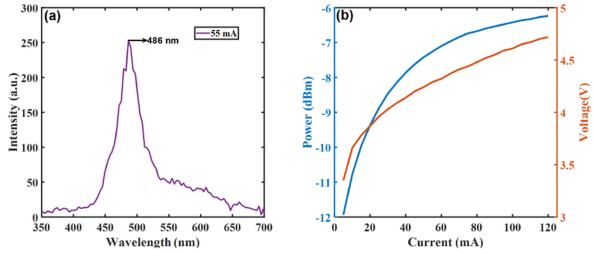

Fig. 3. The (a) spectrum and (b) P-I-V characteristic of the designed 175-μm blue mini-LED.

is filtered by the noise-whitening post-filter with kernel coefficients N can be expressed as (3).

$$z(n) = \mathrm{s}(n) + \sum_{i=1}^{N-1} w_i(n) s(n-l) \tag{3}$$

where $z(n)$ is the n_{th} sample of the output signal after noise-whitening post-filter. After the noise-whitening post-filter, MLSD based on the Viterbi Algorithm (VA) can compensate for the damage of the known ISI caused by the noise-whitening post-filter. When the kernel coefficients of the noise-whitening post-filter are N, the computational complexity of the noise-whitening post-filter is 3N-2 and the computational complexity of the MLSD is 4N. Considering computational complexity and system performance, the N is set as 4 in this work. Finally, the binary sequence was recovered from PAM-4 de-mapping, and BER was calculated.

III. Result

A. Optic-Electro Characteristics of the Mini-LED Device

As shown in Fig. 3(a), the spectrum of the mini-LED is presented at the driving current of 55 mA. Fig. 3(b) shows the voltage and output optical power versus driving current (P-I-V) characteristics of the fabricated mini-LED. The P-I-V curve shows that the threshold driving current of mini-LED is approximately 0.5 mA, the maximum output optical power is about 5.4 dBm. Compared with micro-LED, although the E-O bandwidth of the mini-LED is lower due to a larger RC delay, our design mini-LED can reach higher emitted optical power.

B. 3 dB Modulation Bandwidth Characteristics of the UOWC System

A vector network analyzer (VNA, N5227A, Agilent) measures the system's frequency response under various driving currents. Fig. 4(a) and (c) show the normalized frequency response curves under various driving currents in the 2-m UOWC systems without and with water, respectively. Fig. 4(b) and (d) show the 3 dB modulation bandwidths extracted from Fig. 4(a) and (c). Fig. 4(b) and (d) also show the received optical power under different driving currents of the UOWC systems without and with water, respectively. Fig. 4(b) and (d) show that the 3 dB modulation bandwidth versus the driving current follows the same tendency. The modulation bandwidth of both the UOWC

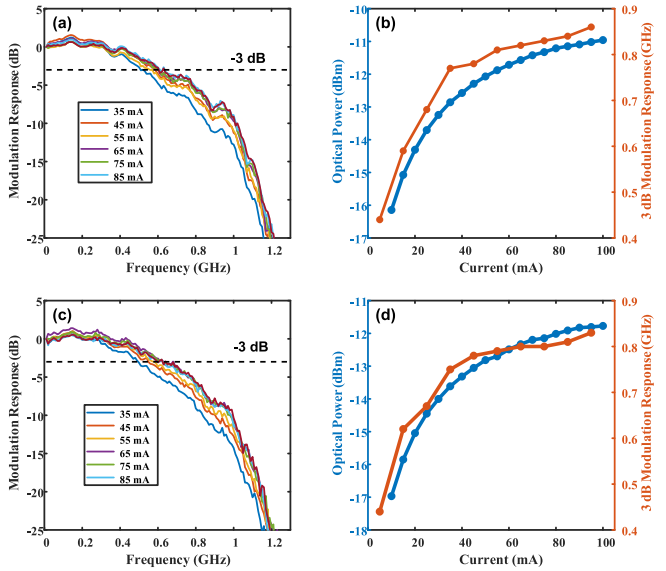

Fig. 4. Normalized modulation responses and 3 dB modulation bandwidth of the UOWC systems (a), (b) without water and (c), (d) with water at various driving currents.

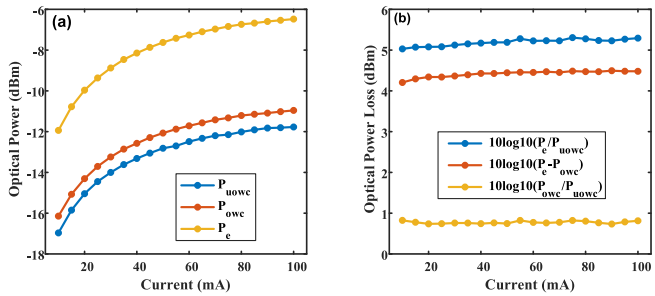

Fig. 5. (a) The optical power of the emitting side and the receiving side under various driving currents over the channel with water or without water. (b) The differences in power between the transmitter and receiver versus driving currents.

systems without and with water approaches saturation as the driving current increases. For the UOWC system with water, the received optical power is slightly smaller than the UOWC system without water, which is mainly caused by the absorption and scattering of water. The 3 dB modulation bandwidth is approximately 580 MHz with the driving current of 45 mA, and the 3 dB modulation bandwidth is about 630 MHz with the driving current of 85 mA.

C. Link Loss and Communication Performance of the UOWC System

In general, the Beer-Lambert law describes the variation of optical power with the transmission distance in the underwater communication channel. The formula is:

$$P = P_0 e^{-cx} \tag{4}$$

where P_0 is the emitted optical power of the blue mini-LED, P is the optical power at a specific distance x, and c is the attenuation coefficient. Fig. 5(a) compares the emitted and received optical

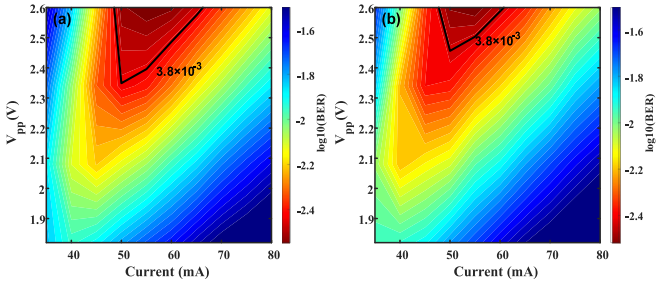

Fig. 6. BER performance as a function of driving current and RF signal modulation depth for the UOWC systems (a) without water and (b) with water.

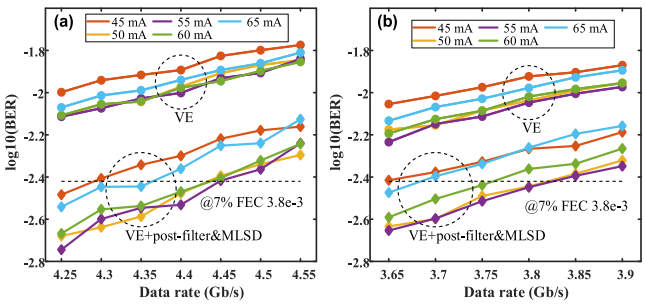

Fig. 7. BERs versus data rate of the UOWC systems (a) without water and (b) with water based on mini-LED with various driving currents from 45 mA to 65 mA, respectively.

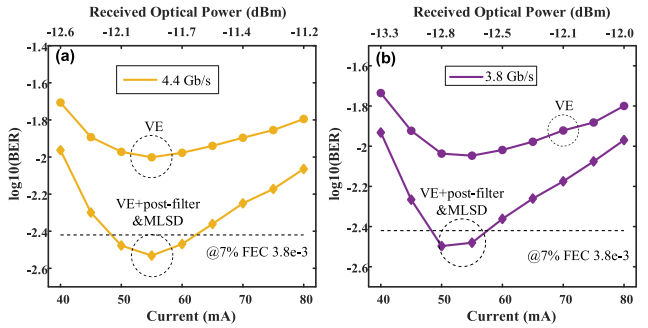

Fig. 8. BERs versus driving current and received optical power for UOWC systems (a) without water and (b) with water, respectively.

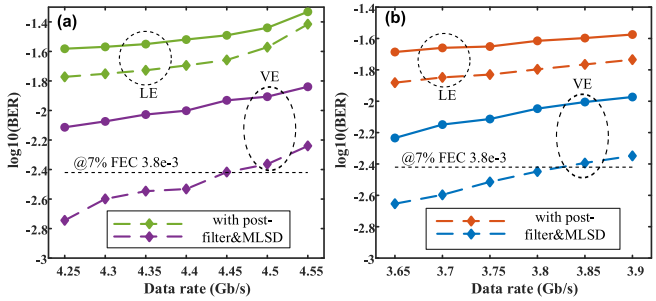

Fig. 9. BER versus data rate for UOWC systems (a) without water and (b) with water based on LE, LE with post-filter and MLSD, VE, and VE with post-filter and MLSD, respectively.

power in the 2-m UOWC systems without and with water. P_e denotes the measured emitted power, P_{owc} and P_{uowc} denote the received power without and with water, respectively. With the increasing driving current, the received optical power becomes saturated. Fig. 5(b) plots the resultant power loss extracted from Fig. 5(a), including the power loss between the transmitter and receiver over the channel without and with water, and the power gap of the received optical power between the UOWC system without and with water. The power loss of the 2-m underwater channel is approximately 0.8 dBm when the driving current of the mini-LED is 45 mA.

By optimizing the number of the memory lengths of VE, we set the memory lengths of the three-order VE as [53, 9, 3], respectively. Thus, the total number of kernel coefficients of the VE is 108.

Fig. 6 shows the contour plots of the BERs as a function of the modulation depth of the RF signal and the driving current of the mini-LED. Fig. 6(a) presents the BER performance with the data rate of 4.4 Gb/s of the UOWC system without water. Fig. 6(b) shows the BER performance with the data rate of 3.8 Gb/s of the UOWC system with water. The black line is marked as the 7% FEC threshold of 3.8×10^{-3} in Fig. 6, which presents the optimal operating region of modulation depth and driving current. The system has the best BER when the driving current is about 45 mA $\sim$ 65 mA, and the modulation depth is about 2.5 Vpp $\sim$ 2.6 Vpp. Therefore, the following experiments adopt the optimal 2.6 Vpp as the modulation depth for the UOWC systems without and with water.

Fig. 7 shows the BER performance versus data rates under different driving currents. Since the bandwidth limitation of the UOWC system (3dB bandwidth of 580 MHz only) is severe, the VE combined noise-whitening post-filter with MLSD improves the BER performance significantly compared to the VE only. With the VE followed by post-filter plus MLSD, Fig. 7(a) shows the BER can reach a 7% HD-FEC threshold at 4.4 Gb/s in the 2-m UOWC system without water with the driving current between 50 mA and 60 mA. Fig. 7(b) shows that the data rate of 3.8 Gb/s can be obtained below the 3.8e-3 over the 2-m channel with water with the driving current between 50 mA and 55 mA, which is the highest data rate of PAM-4 UOWC systems based on a single-pixel LED.

Fig. 8 shows the BER as a function of the driving currents ranging from 40 mA to 80 mA. The received optical power at the respective driving currents is also shown together. The results show that there is an optimal current to obtain the best BER performance. This result is consistent with the contour plots in Fig. 6. For the UOWC system without water, the PAM-4 signal with the data rate of 4.4 Gb/s reaches the lowest BER at the driving current of 55 mA, whereas the UOWC system with water has the lowest BER at 50mA with the obtained data rate of 3.8 Gb/s. Furthermore, the performance improvement provided by noise-whitening post-filter with MLSD confirmed that a successful compensation of the ISI is achieved.

Fig. 9 shows the measured BER of PAM-4 over different equalization schemes. The feed-forward LE, the VE, and these two types of equalizers followed by noise-whitening post-filter

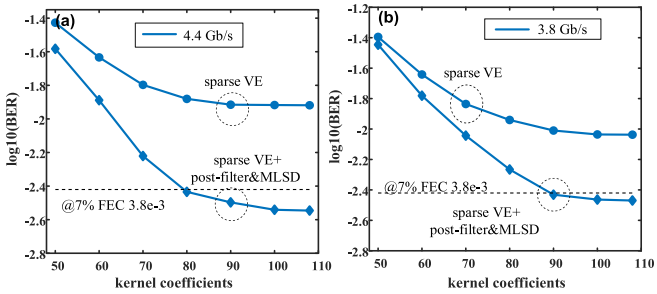

Fig. 10. BER performances versus the kernel coefficients of the sparse VE for UOWC systems (a) without water and (b) with water.

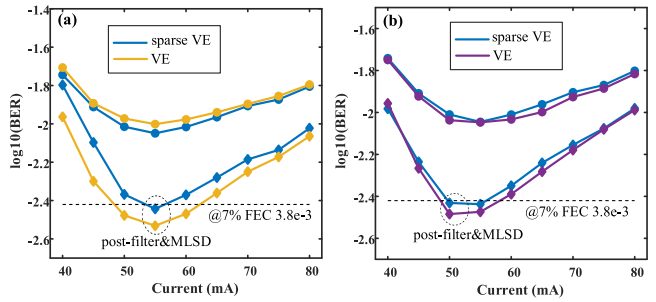

Fig. 11. BER performances versus driving current for UOWC system (a) without water and (b) with water.

and MLSD are studied for performance comparison. The kernel coefficients of the feed-forward LE are 53. The training-symbol-based recursive least squares (RLS) algorithm is used to update the kernel coefficients. In the UOWC system, the system nonlinearity penalty is evident due to the optoelectronic devices. Therefore, the VE achieves a significant system performance improvement compared to the LE, whether with the noise-whitening post-filter and MLSD or without it. Fig. 9 also shows that noise-whitening post-filter and MLSD provide further performance gain, which can be attributed to successful compensation of bandwidth limitation for the UOWC systems without and with water.

The VE memory lengths are set as (53 93), so the total number of the coefficients of the VE is 108. We adopt the TPCA to remove the less significant kernel coefficients of the VE. Fig. 10(a) and (b) show the BER performance as the function of the kernel coefficients of the sparse VE based on the TPCA in the UOWC systems without water and water, respectively. The driving currents of the UOWC system with and without water are set as 55 mA and 50 mA, respectively. Fig. 10(a) shows that when the kernel coefficients of the sparse VE are not less than 80, the BER can still reach a 7% HD-FEC threshold over the 2-m channel without water at the date rate of 4.4 Gb/s. In Fig. 10(b), the 3.8 Gb/s PAM-4 signal is transmitted over the 2-m underwater channel with the BER of 3.7×10^{-3} using the 90 kernel coefficients of the sparse VE.

In Fig. 11, the driving current configuration is the same as in Fig. 10. In the UOWC system without water, the number of the coefficients of the sparse VE is 80, whereas it is 90 in the UOW–C system with water. Fig. 11 shows the BER as a function of the driving current in the UOWC system. In the UOWC without water, when the data rate is 4.4 Gb/s, the BER is below 3.8×10^{-3} with the aid of the sparse VE combined noise-whitening post-filter with MLSD. In the UOWC system with water, the BER of the 3.8 Gb/s PAM-4 signal is 3.4×10^{-3} using the traditional VE and noise-whitening post-filter plus MLSD, whereas the BER of the sparse VE is 3.7×10^{-3}. Therefore, the optimized VE based on the TPCA has a slight BER performance degradation compared to the traditional VE with the gain of the complexity reduction.

Although the sparse VE has the capability of reducing computational resources, it still has relatively high and comparable complexity compared with Neural-Network-based equalizers [32]–[34]. To achieve a hardware-feasible scheme, digital pre-emphasis will be considered in the transmitter. Consequently, the required kernel coefficients of the equalizer can be reduced in the receiver. This implementation will be investigated and discussed in our subsequent research work.

IV. Conclusion

In this paper, the PAM-4 UOWC system without and with water based on a high-bandwidth 175-μm mini-LED has been proposed and experimentally demonstrated over a 2-m transmission distance. We adopt the VE combined noise-whitening post-filter with the MLSD scheme to effectively compensate for the linear and nonlinear impairments in the PAM-4 UOWC system. We achieve the data rate of 4.4 Gb/s for the UOWC system without water with the BER of 2.8×10^{-3} at the driving current of 50 mA, and the data rate of 3.8 Gb/s for the UOWC system with water with the BER of 3.3×10^{-3} and 55 mA, respectively. In the UOWC system without water, when the kernel coefficients of the sparse VE based on TPCA are 80, the BER of the 4.4 Gb/s PAM-4 signal is 3.6×10^{-3}. In the UOWC system with water, the BER of the 3.8 Gb/s PAM-4 signal over the 2-m channel with water is 3.7×10^{-3} when the kernel coefficients of the sparse VE based on TPCA are 90. Therefore, the UOWC system assisted by the sparse VE has an acceptable penalty of BER performance. To the best of our knowledge, over 2-m underwater transmission distance, this is the highest data rate record of 3.8 Gb/s, and rate-distance product record of 7.6 Gb/s·m among the UOWC systems using PAM-4 based on a single-pixel LED and a single APD.

References

[1] Z. Zeng, S. Fu, H. Zhang, Y. Dong, and J. Cheng, "A survey of underwater optical wireless communications," *IEEE Commun. Surv. Tut.*, vol. 19, no. 1, pp. 204–238, Jan.–Mar. 2017.
[2] H. Kaushal and G. Kaddoum, "Underwater optical wireless communication," *IEEE Access*, vol. 4, no. 1, pp. 1518–1547, 2016.
[3] M. Stojanovic, "Recent advances in high-speed underwater acoustic communications," *IEEE J. Ocean. Eng.*, vol. 21, no. 2, pp. 125–136, Apr. 1996.
[4] G. Cossu, "Recent achievements on underwater optical wireless communication," *Chin. Opt. Lett.*, vol. 17, no. 10, pp. 54–60, 2019.
[5] L. Johnson, R. Green, and M. Leeson, "A survey of channel models for underwater optical wireless communication," in *Proc. 2nd Int. Workshop Opt. Wireless Commun.*, 2013, pp. 1–5.
[6] C. Li *et al.*, "A 5 m/25 Gbps underwater wireless optical communication system," *IEEE Photon. J.*, vol. 10, no. 3, Jun. 2018, Art. no. 7904909.

[7] H. Chen *et al.*, "Toward long-distance underwater wireless optical communication based on a high-sensitivity single photon avalanche diode," *IEEE Photon. J.*, vol. 12, no. 3, Jun. 2020, Art. no. 7902510.
[8] Y. Zhou *et al.*, "Common-anode LED on a Si substrate for beyond 15 Gbit/s underwater visible light communication," *Photon. Res.*, vol. 7, no. 9, pp. 1019–1029, 2019.
[9] G. N. Arvanitakis *et al.*, "Gb/s underwater wireless optical communications using series-connected GaN micro-LED arrays," *IEEE Photon. J.*, vol. 12, no. 2, pp. 1–10, Apr. 2020.
[10] Z. Wei *et al.*, "2 Gbps/3 m air–underwater optical wireless communication based on a single-layer quantum dot blue Micro-LED," *Opt. Lett.*, vol. 45, no. 9, pp. 2616–2619, 2020.
[11] Y. Song *et al.*, "Experimental demonstration of MIMO-OFDM underwater wireless optical communication," *Opt. Commun.*, vol. 403, no. 1, pp. 205–210, 2017.
[12] P. Tian *et al.*, "High-speed underwater optical wireless communication using a blue GaN-based micro-LED," *Opt. Exp.*, vol. 25, no. 2, pp. 1193–1201, 2017.
[13] I. Lu and Y. Liu, "205 Mb/s LED-based underwater optical communication employing OFDM modulation," in *Proc. OCEANS - MTS/IEEE Kobe Techno-Oceans*, 2018, pp. 1–4.
[14] N. Chi, Y. Zhao, M. Shi, P. Zou, and X. Lu, "Gaussian kernel-aided deep neural network equalizer utilized in underwater PAM8 visible light communication system," *Opt. Exp.*, vol. 26, no. 20, pp. 26700–26712, 2018.
[15] M. Kong *et al.*, "Underwater wireless optical communication using an arrayed transmitter/receiver and optical superimposition-based PAM-4 signal," *Opt. Exp.*, vol. 26, no. 3, pp. 3087–3097, 2018.
[16] P. Zou, Y. Liu, F. Wang, and N. Chi, "Mitigating nonlinearity characteristics of gray-coding square 8QAM in underwater VLC system," in *Proc. Asia Commun. Photon. Conf.*, 2018, pp. 1–3.
[17] F. Wang, Y. Liu, F. Jiang, and N. Chi, "High speed underwater visible light communication system based on LED employing maximum ratio combination with multi-pin reception," *Opt. Commun.*, vol. 4, no. 25, pp. 106–112, 2018.
[18] J. Li, F. Wang, M. Zhao, F. Jiang, and N. Chi, "Large-coverage underwater visible light communication system based on blue LED employing equal gain combining with integrated pin array reception," *Appl. Opt.*, vol. 58, no. 2, pp. 383–388, 2019.
[19] M. Chen, P. Zou, L. Zhang, and N. Chi, "Demonstration of a 2.34 Gbit/s real-time single silicon-substrate blue LED-based underwater VLC system," *IEEE Photon. J.*, vol. 12, no. 1, Feb. 2020, Art. no. 7900211.
[20] Z. Zhang *et al.*, "Over 700 MHz –3 dB bandwidth UOWC system based on blue HV-LED with T-bridge pre-equalizer," *IEEE Photon. J.*, vol. 11, no. 3, Jun. 2019, Art. no. 7903812.
[21] J. Lian, M. Noshad, and M. Brandt-Pearce, "Comparison of optical OFDM and M-PAM for LED-based communication systems," *IEEE Commun. Lett.*, vol. 23, no. 3, pp. 430–433, Mar. 2019.
[22] B. Zhuang, C. Li, N. Wu, and Z. Xu, "First demonstration of 400Mb/s PAM4 signal transmission over 10-meter underwater channel using a blue LED and a digital linear pre-equalizer," in *Proc. Conf. Lasers Electro-Opt.*, 2017, pp. 1–2.
[23] W. Liu *et al.*, "PAM-4 and PAM-8 transmission in visible light communication system employing volterra kernels based feed forward equalizer," in *Proc. Asia Commun. Photon. Conf.*, 2017, pp. 1–3.
[24] J. Li, E. Tipsuwannakul, T. Eriksson, M. Karlsson, and P. A. Andrekson, "Approaching Nyquist limit in WDM systems by low-complexity receiver-side duobinary shaping," *J. Lightw. Technol.*, vol. 30, no. 11, pp. 1664–1676, 2012.
[25] J. Pan and C.-H. Cheng, "Nonlinear electrical compensation for the coherent optical OFDM system," *J. Lightw. Technol.*, vol. 29, no. 2, pp. 215–221, 2011.
[26] W.-J. Huang *et al.*, "93% complexity reduction of Volterra nonlinear equalizer by $\ell 1$ -regularization for 112-Gbps PAM-4 850-nm VCSEL optical interconnect," in *Proc. Opt. Fiber Commun. Conf.*, 2018, pp. 1–3.
[27] Z. Yang, S. Fu, M. Tang, Y. Wang, and Y. Qin, "Optimized volterra filter equalizer based on weighted principal component analysis for IM-DD transmission," *Opt. Lett.*, vol. 46, no. 7, pp. 1680–1683, 2021.
[28] Z. Wan *et al.*, "64-Gb/s SSB-PAM4 transmission over 120-km dispersion-uncompensated SSMF with blind nonlinear equalization, adaptive noise-whitening postfilter and MLSD," *J. Lightw. Technol.*, vol. 35, no. 23, pp. 5193–5200, 2017.
[29] L. Wang, D. Yang, Z.-B. Hao, and Y. Luo, "Metal–organic–vapor phase epitaxy of InGaN quantum dots and their applications in light-emitting diodes," *Chin. Phys. B*, vol. 24, no. 6, pp. 67303–67313, 2015.
[30] L. Wang *et al.*, "1.3 GHz E-O bandwidth GaN-based micro-LED for multi-gigabit visible light communication," *Photon. Res.*, vol. 9, no. 5, pp. 792–802, 2021.
[31] T. Wettlin, S. Calabrò, T. Rahman, J. Wei, N. Stojanovic, and S. Pachnicke, "DSP for high-speed short-reach IM/DD systems using PAM," *J. Lightw. Technol.*, vol. 38, no. 24, pp. 6771–6778, 2020.
[32] Z. Wan *et al.*, "Nonlinear equalization based on pruned artificial neural networks for 112-Gb/s SSB-PAM4 transmission over 80-km SSMF," *Opt. Exp.*, vol. 26, no. 8, pp. 10631–10642, 2018.
[33] A. G. Reza and J. K. Rhee, "Nonlinear equalizer based on neural networks for PAM-4 signal transmission using DML," *IEEE Photon. Technol. Lett.*, vol. 30, no. 15, pp. 1416–1419, Aug. 2018.
[34] Y. Xi, C. Wang, X. Miao, M. Bi, and W. Hu, "High-efficient equalizer based on the simplified deep neural network for 56Gb/s/λ PAM-4 in C-band 10G DML-based short reach system," in *Proc. Asia Commun. Photon. Conf. Int. Conf. Inf. Photon. Opt. Commun.*, 2020, pp. 1–3.